HHS Public Access

Author manuscript

Ann Eye Sci. Author manuscript; available in PMC 2023 August 24.

Published in final edited form as:

Ann Eye Sci. 2022 March 15; 7: . doi:10.21037/aes-21-25.

Comparison between sodium iodate and lipid peroxide murine models of age-related macular degeneration for drug evaluation—a narrative review

Soo-Young Kim[1,2], **Haohua Qian**[3]

[1]Department of Pharmaceutics, Department of Biology, Virginia Commonwealth University, Richmond, VA, 23298, USA;

[2]Center for Nanomedicine, Wilmer Eye Institute, Department of Ophthalmology, Johns Hopkins University of Medicine, Baltimore, MD, 21287, USA;

[3]Visual Function Core, National Eye Institute, National Institutes of Health, Bethesda, Maryland, USA.

Abstract

Objective: In this review, non-transgenic models of age-related macular degeneration (AMD) are discussed, with focuses on murine retinal degeneration induced by sodium iodate and lipid peroxide (HpODE) as preclinical study platforms.

Background: AMD is the most common cause of vision loss in a world with an increasingly aging population. The major phenotypes of early and intermediate AMD are increased drusen and autofluorescence, Müller glia activation, infiltrated subretinal microglia and inward moving retinal pigment epithelium cells. Intermediate AMD may progress to advanced AMD, characterized by geography atrophy and/or choroidal neovascularization. Various transgenic and non-transgenic animal models related to retinal degeneration have been generated to investigate AMD pathogenesis and pathobiology, and have been widely used as potential therapeutic evaluation platforms.

Methods: Two retinal degeneration murine models induced by sodium iodate and HpODE are described. Distinct pathological features and procedures of these two models are compared. In addition, practical protocol and material preparation and assessment methods are elaborated.

Correspondence: Soo-Young Kim, Ph.D. 616 Coral Reef Dr. Gaithersburg, Maryland, USA. gungil@korea.ac.kr.

Authors' Contributions: (I) Conception and design: SYK; (II) Administration support: SYK; (III) Provision of study materials or patients: Not applicable; (IV) Collection and assembly of data: Not applicable (V) Data analysis and interpretation: Not applicable; (VI) Manuscript writing: All authors; (VII) Final approval of manuscript: All authors.

Reporting Checklist: The authors have completed the Narrative Review reporting checklist.

Conflicts of Interest: Both authors have completed the ICMJE uniform disclosure from. The authors have no financial conflict of interest to declare, however the author (SYK) was an employee of ExosomePlus, Inc. (South Korea). The authors have no other conflicts of interest to declare.

Ethical Statement: The authors (SYK, HQ) are accountable for all aspects of the work in ensuring that questions related to the accuracy or integrity of any part of the work are appropriately investigated and resolved.

Conclusion: Retina degeneration induced by sodium iodate and HpODE in mouse eye resembles many clinical aspects of human AMD and complimentary to the existent other animal models. However, standardization of procedure and assessment protocols is needed for preclinical studies. Further studies of HpODE on different routes, doses and species will be valuable for the future extensive use. Despite many merits of murine studies, differences between murine and human should be always considered.

Keywords

Retina degeneration; Retinal pigment epithelium; Photoreceptor; Microglia

1. Introduction

Age-related macular degeneration (AMD) is a neurodegenerative retina disorder of which the early and intermediate forms are characterized by an increasing number and size of drusen and drusenoid deposits, Müller glia activation (1–3), infiltrated subretinal microglia (3,4), autofluorescence (5–7) and inward moving retinal pigment epithelium cells (8). Advanced AMD often exhibits geographic atrophy (GA) and choroidal neovascularization (CNV). In this review, GA is referred as the Dry form and CNV as the Wet form of AMD. The current available treatment for early/intermediate AMD refers to the Age-Related Eye Disease Study (AREDS) (9,10), dietary supplements consisting of a calibrated blend of anti-oxidants. Intravitreal injections of vascular endothelial growth factor (VEGF) inhibitors are indicated for CNV (11), which however may accelerate the occurrence of GA (12,13), for which there are no FDA approved drugs.

As the aging population is globally increasing, the research and drug development for aging-related diseases, including AMD, are important, given that the AMD population is estimated to be ~196 million and to reach ~288 million by 2040 (14). Animal research has helped us to understand disease pathogenesis and pathobiology, although animal disease models have limitations being not like humans. The retina of rodents has no macula and has different subtypes of retinal neurons from humans (15). To date, researchers have investigated and developed genetic (Table 1) and non-genetic AMD murine models (Table 2). The genetic mouse model includes juvenile macular dystrophy, metabolic pathway, inflammatory and oxidative stress genes. The table 1 displays that inflammation is essential part to drive disease progression especially into the wet form. The phenotypes of all these genetic models get severer by light, fat diet and/or laser. Currently, we do not have a typical murine model for Dry AMD, whereas laser-induced and VEGF-A^{high} CNV models are typical for Wet AMD studies (16,17). Recently, a laser-induced Dry AMD model was reported (18) and is waiting for a deeper evaluation. Light damage is a classical model for retinal degeneration, and is still recommended and used for the preclinical study of Dry AMD (e.g., Guideline of Korea National Institute of Food and Drug Safety Evaluation for the Eye Health Functional Food Preclinical Studies). Depending on the source of lamps and wave lengths of lights, light induces damage of either photoreceptors or RPE, or both: usage of fluorescent lamps has induced photoreceptor damage rather than RPE, whereas usage of light-emitting diode (LED) lamps and source of blue light induce RPE degeneration (19,20). A number of pharmacologically induced animal models of Dry AMD have been

reported, including: peptide amyloid beta (21,22), metals (23–25), sodium iodate (26–34), n-methyl n-nitrosourea (MNU) (35,36), 13(S)-hydroperoxy-9Z, 11E-octadecadienoic acid (HpODE) (2,37,38), and cisplatin (39–41), given via intravitreal, subretinal and/or systemic injections. In addition, immunization model using carboxyethylpyrrole (CEP) adducts has been applicable (42,43). The purpose of this review is to describe, compare and discuss the details of murine retina degeneration models induced by sodium iodate or lipid hydroperoxide HpODE and provide an example of the practical protocols commonly used to induce retina degeneration with these methods. For the detailed description of all other genetic and non-genetic AMD models, several review articles on these topics (44–46) are available. We present the following article in accordance with the Narrative Review reporting checklist.

2. Phenotype description of retina degeneration induced by sodium iodate or lipid peroxides (HpODE)

Sodium iodate-induced retina degeneration has been widely applied to different animal species, including rabbit, sheep, dog (47) and mouse via the administration routes of tail (26) or femoral vein (48), retro-orbital venous sinus (30), intraperitoneal (34), subretinal (29) and/or intravitreal (28) injections (Figure 1). Systemic injection of sodium iodate induces acutely RPE degeneration within a day, and increasing photoreceptor degeneration, followed by outer nuclear layer rosettes formation, but no significant damage in other retinal layers (49) (Figure 2). On the other hand, lipid peroxides were applied to *New Zealand* rabbits (38) and *Sprague-Dawley (SD)* rats via the administration routes of intravitreal and subretinal injections (2,37). Subretinal administration of linoleic acid peroxide, (HpODE) induces acute local degeneration of RPE and photoreceptor around and at the injection site, and the degeneration is peripherally expanded through all retina layers, and finally induces CNV around 3 weeks post-injection (2,37) (Figure 2).

2.1 Sodium iodate

Depending on the administration route of sodium iodate, the features of retina degeneration are different: a systemic injection induces mainly rapid RPE degeneration, while subretinal injection causes local loss of both RPE and photoreceptors (29), whereas intravitreal injection induces photoreceptor, rather than RPE, degeneration (28). The concentration of sodium iodate generally used is between 20 and 100 mg/kg; 20–30 mg/kg via retro-orbital injection is enough to trigger retina degeneration (30), whereas 40–50 mg/kg is generally acceptable for systemic intravenous (i.v.) and intraperitoneal (i.p.) injections (26,34). The proper sodium iodate amount for subretinal injection can be 5 μg in1 μl for rats (29) and 1 to 50 μg in 100 μl for pigs (50). Thus injected rats displayed focal loss of RPE and photoreceptors, but no defects in inner retina. In pigs, 1 μg sodium iodate injection induced the same focal loss of RPE and photoreceptors and no inner retina defects, but 50 μg induced the degeneration of all retinal layers (50). Interestingly, the intravitreal injection of sodium iodate (300 or 400 μg, 50 μl injection) in rabbits induced only retinal, but no RPE degeneration (28) (Table 3). Although there are intensive studies on sodium iodate-induced retinal degeneration, relatively few compared different murine strains. For instance, it is known that *C57BL/6J* mice have a higher superoxide production than *129S6/SvEvTac* mice

(51) and that *C57BL/6J* mice respond severely to sodium iodate than *BALB/C* mice, when measured by electroretinogram (ERG) responses (34). Further, it is worth noting that sodium iodate-induced retina degeneration is partially reversible (26,32,52). Müller neurogenesis (53) and proliferating cells (32,53) are detected at early stages after damage, and areas with recovered RPE (26) are observed at later stages, around a month post-injection.

2.2 Lipid peroxides

Lipid peroxides (linoleic, linolenic, arachidonic, docosahexaenoic acids) were first applied to rabbits via intravitreal injection. Nineteen mg of linoleic peroxides abolished a- and b-wave ERG responses by 7 days post-injection, and the same amounts of linolenic and docosahexaenoic acid peroxides abolished a- and b-wave ERG responses by 14 days post-injection, whereas arachidonic peroxide injection only slightly reduced a- and b-wave ERG responses (38) (Table 4). The subretinal injection of commercial linoleic acid peroxide, HpODE (30 μg), into the eyes of *SD* rats induced extended retina and RPE degeneration, retina inflammation, oxidative stress, and, finally, CNV by 3 weeks post-injection (2,37) (Figure 2). It is unclear whether the subretinal injections of linolenic, docosahexaenoic acid peroxides, and the intravitreal injection of lipid peroxides may also induce CNV.

3. Practical protocol description of retina degeneration induced by sodium iodate and lipid peroxide HpODE

Sodium iodate (10 to 50 mg/kg) were peritoneally injected into the mice of *BALB/C* and *C57BL/6J* (8–10 weeks, 20–30 g) or *SD* (8–10 weeks, 200–350g) rats for the observation of retinal degeneration, whereas HpODE was injected into the subretinal space of *SD* rats (6–8 weeks, 150–250 g).

Sodium iodate from Sigma (catalog number: 71702–25 g) and lipid peroxide HpODE from Cayman Chemical (catalog number: 48610–500 μg) were used in these studies. Compounds of sodium iodate and HpODE are summarized in Table 5.

The stock solution of sodium iodate was prepared at a concentration of 20 mg/ml in sterile saline, and aliquots were stored at −20°C. The stock of sodium iodate was replaced every 6 months, because a diminished effect was observed overtime. The stock solution was further diluted with saline and the diluted solution was injected into mice and rats at a standard dose (Table 6).

The HpODE solution (15 μg/1 μl) was prepared by dissolving HpODE in ethanol. The ethanol solution was then evaporated by nitrogen gas streaming and HpODE reconstituted with 0.02 M sodium borate buffer at the desired concentration (pH 9.0), kept on ice, and used within 24 hours. For the subretinal injection of HpODE, a rat was anesthetized with ketamine and xylazine (see below), pupil dilated with tropicamide, and cornea topically anesthetized by proparacaine hydrochloride. The HpODE solution was then injected into the subretinal space by a capillary micropipette, using a PL1–100A injector guiding the capillary into a hole previously done by a tiny needle (30 ½ gauge).

The detailed materials for HpODE subretinal injection are summarized in Table 7, and the practical procedures of sodium iodate peritoneal injection, and HpODE subretinal injection were done as following.

3.1. Procedure for sodium iodate i.p. injection

1. Dilute the stock sodium iodate solution (20 mg/ml) to make a 2 mg/ml sodium iodate saline solution.
2. Weigh mice or rats to determine their body weight and establish the dose to be injected.
3. Inject i.p. the sodium iodate (Table 7) into mice or rats.
    - The peritoneal injection of sodium iodate at high dose (40 and 50 mg/kg) induces RPE degeneration from center to peripheral areas, whereas low dose (10 and 20 mg/kg) induces only central RPE degeneration in *BALB/C* mice.
    - Sodium iodate may evoke allergic symptoms in the operator: hives, itching, rashes, burning sensation, asthma, breathing difficulties, etc. Put on gloves, a mask, lab coat and goggles to protect yourself from sodium iodate.

3.2 Procedure of HpODE subretinal injection

3.2.1 Material preparation for HpODE subretinal injection

Sodium borate buffer solution (0.02M, pH9.0) for HpODE reconstitution: Dissolve 12.4 mg of boric acid in 5 ml of water, adjust to pH 9.0 with NaOH and add water to 10 ml. Sterilize by filtration through 0.2 μm filters the 0.02M sodium borate buffer solution before use.

Micropipette preparation: Pull 100 mm glass capillary micropipettes (diameter 25 to 30 μm) using P-80 Flaming micropipette puller (setting: Heat-950, Pull 44, Vel 30, Time 70) and cut off the pulled pipettes with razor, if needed.

Anesthetic solution for rats: Add 1.1 ml of xylazine (100 mg/ml) into 10 ml ketamine solution (100 mg/ml).

Inject subcutaneously (s.c.) or i.p. the mixed solution of ketamine and xylazine (100 μl per 100 g rat) into SD rats (6–8 weeks). 150 to 200 μl solution is enough for 6–8 weeks old rats.

or

Add 2.5 ml of xylazine (20 mg/ml) into 10 ml ketamine solution (50 mg/ml).

Inject (s.c. or i.p.) the mixed solution of ketamine and xylazine (200 μl per 100 g rat) into SD rats (6–8 weeks). 300 to 500 μl solution will be enough for 6–8 weeks old rats.

- Depending on Countries and local regions, the available commercial concentration of ketamine and xylazine may be different. Therefore, the mixed

solution should be re-calculated based on the available concentrations of each single solution so to inject 80–100 mg/kg ketamine and 5–10 mg/kg xylazine per rat.

Lipid formulation: Evaporate the ethanol from HpODE under nitrogen gas and dilute the residual pellet in sterile 0.02 M sodium borate buffer (pH 9.0), keep on ice and use immediately, or practically within 8 hours.

3.2.2. HpODE subretinal injection—Before starting any procedure, set up the working surgery place and a surgical microscope (check focusing and controlling of the foot pedal), set up a picoinjector (PLI-100A) and micropipettes filled with HpODE (30 μg, 2 μl), set up an injector (pressure 40 psi, injection volume 2 μl, adjust injection time: 0.06 to 0.2 sec). The procedure of HpODE subretinal injection should be done by three operators consisting of a surgeon and two assistant staffs. The surgeon focuses on subretinal injection, while the staff helps with anesthesia (steps 1 to 3 below), and another staff takes care of the rest: tapping and centrifuging HpODE solution before use, applying GONAK solution (hypromellose 2.5% for gonioscopy) to the eye (step 11 below), injector operation, recording, etc. Keep the HpODE solution on ice during the surgical procedure.

1. Anesthetize rats with s.c. or i.p. injection of ketamine and xylazine.
2. Drop the tropicamide solution into both eyes.
3. Trim whiskers.
4. Put the rat on a working surgery area.
5. Apply Duratears (or similar): a lubricating eye ointment on the non-operated eye.
6. Add one drop of Mydfrin (phenylephrine hydrochloride) on the eye to be operated.
7. Add one drop of proparacaine or tetracaine solution on the eye to be operated.
8. Clean the eye with a sterile swab.
9. Make a tiny hole in the nasal quadrant with a needle (30 ½ gauge), about 1 mm outside the corneal limbus.
10. Insert a micropipette containing the HpODE solution into the eye through the hole into the subretinal region
11. Apply a drop of GONAK to cover the eyeball.
12. Find an injection site, avoiding choroid vessels.
13. Inject 2 μl (HpODE 30 μg) into the subretinal space and check to see a bleb or retinal detachment, so that a good procedure is ensured.
14. Record the injection location on a surgical note (Supplemental Figure S1).
15. Repeat steps for the other eye of the rat.
16. Repeat all steps for other rats.

- Exclude eyes with subretinal hemorrhage, which might develop CNV regardless of HpODE injection success.
- HpODE is also a health hazard. It may cause cough, headache, heart and liver damage, etc.

4. Assessment of retina degeneration in murine models

In degenerative conditions of the outer retina, the dysfunction and loss of RPE and photoreceptors are the main causes of vision impairment. To assess outer retina degeneration, non-invasive ophthalmic analyses such as the fundus imaging, optical coherence tomography and electroretinogram (ERG) can be applied, as well as other invasive assessment methods, as described below. In this section, ERG as a non-invasive measurement is described, and the invasive assessment of retinal thickness, photoreceptor loss, outer nuclear layer folds, RPE loss, subretinal microglia infiltration, and expression of inflammatory, oxidative and cell death genes are discussed. Moreover, the benefits of the sclerochoroid/RPE/retina whole mount application to observe the flat view of the disorganized subretinal and outer nuclear layers (49), and the infiltrated subretinal microglia (54,55) are discussed.

4.1. ERG

Visual dysfunction is considered to be an early physiological marker, and a sensitive indicator compared to morphological evaluation. The a- and b-waves of dark-adapted (scotopic) ERG represent the primary activities of photoreceptors and bipolar cells, respectively (Figure 3A). Light-adapted (photopic) ERG can be used to probe cone photoreceptor mediated activities in the retina. Glial cells provide support and nourishment to retinal neurons, and are essential for photoreceptor function and survival. Alterations in glia function could also indirectly modify ERG a- and b-waves (56,57). In addition, glia activity contributes to the formation of ERG c-wave response (3,58), together with RPE activity which represents two major components with opposite polarity. In contrast to a- and b-wave response, often elicited with flashlight stimuli, slow response of c-wave (usually peaking at 3–5 seconds after light onset) is commonly elicited by a long light stimulus (3,59,60). In rodent models of retina degeneration, such as sodium iodate and HpODE, ERG response of a- and b-waves is well-correlated to morphological degeneration in retina (2,34,38). Retina degeneration induced by intravitreal and subretinal HpODE is relatively slow: an extensive damage is detectable after 2–3 weeks (2), compared with systemic sodium iodate. ERG response also decreases slowly (38), compared to the sudden reduction of ERG observed within a week after sodium iodate injection (40 to 50 mg/kg) (26,31,61,62). In drug efficacy tests, ERG response in retinal degeneration is considered to be more sensitive than morphological evaluation, but both of them are, ultimately, correlated.

4.2. Retina thickness quantification

The thickness of the total retina and each retinal layer in murine models is quantified in histological sections by measuring its length in vertical paraffin sections or counting nuclei in a column of layer. The thickness is measured at a specific region (e.g., 300 to 500 μm

away) or a specific length away (e.g., every 150, 250, 300 μm away) from the center of the optic nerve head (26,31,34) (Figure 3B).

4.3. Photoreceptor loss and rosettes quantification

Photoreceptor loss is reflected by the thickness of whole retina, outer nuclear layer, and/or photoreceptor outer/inner segments (34), and the same measurement method described above in retina thickness quantification is applied. The fluorescent intensity of opsin expressions – Rho, S-opsin, M-opsin - is further observed and measurable by immunofluorescence staining in sectioned and whole mount retinas (28,34,63). In sodium iodate model of retina degeneration, number and area of photoreceptor folds/rosettes are measurable in retinal sections (48) and sclerochoroid/RPE/retina whole mounts, and the representative images of the rosettes induced by sodium iodate in sclerochoroid/RPE/retina whole mounts can be seen in a paper published in this journal (49) (Figure 3C).

4.4. RPE loss quantification

RPE loss in rodents is detectable in histology sections of both pigmented and non-pigmented murine retinas. In the pigmented murine retina, RPE loss, swelling and mis-location are detected easily by lost, swelling and mis-located pigments whereas in the non-pigmented murine retina, loss, swelling and mis-location are observed with pale-tinted and big sized RPE nuclei. In addition, the immunofluorescence staining of RPE biomarkers - RPE65, ZO-1 and GLUT1- are also applicable in retina sections and whole mounts (2,26,29,32,34,63,64). Furthermore, fluorescence of phalloidin stained retina allows the counting of the number of outlined RPE cells in whole mounts (2,30) (Figure 3D).

4.5. Subretinal macrophages/microglia quantification

In outer retinal degeneration, the subretinal layer may include migrated photoreceptors, RPE cells, and microglia/macrophages. The nuclei of these cells in the subretinal layer are recognizable and countable in histology sections (3). The morphology and size of these nuclei are different from each other (3,54). The genetically fluorescence-labeled macrophages/microglia mice (e.g., CX3CR1-GFP) could also be used (65), and the immunofluorescence staining of macrophages/microglia - Iba1, CD11b - detects subretinal infiltrated microglia in retina sections and whole mounts (3,54,55), amenable for quantitative analysis.

4.6. Sclerochoroid/RPE/retina whole mount

Sclerochoroid/RPE/retina whole mount and imaging have recently been developed in mice and ferrets (55,66). The method allows to observe intact and integral subretinal and neighboring layers in the degenerative outer retina (Figure 4). The detailed protocol was previously published (54), and the method is applicable for the integral observation of the infiltrated subretinal microglia, and outer nuclear layer rosettes (49). Classic whole mount method viewing either the neural retina or the RPE side, the subretinal microglia appear separate, depending on their location, and a part of microglia neurites are on the RPE side and another part are visible at the retina side of the whole mount, so that it is hard to figure out the actual number of the subretinal microglia. Moreover, this tissue

separation causes additional damage to already degenerated areas. Even in normal retinas, the separation between RPE and retinal tissue could cause artificial scars in RPE microvilli and photoreceptor segments (55). Thus, the non-separate sclerochoroid/RPE/retina whole mount and imaging method could provide reliable horizontal images, especially of the subretinal and neighboring layers. It is worth mentioning that all layers in the mouse retina are accessible by confocal microscopy in the non-separate whole mount method (54), but in the rat, the imaging of subretinal layer is not accessible (Zeiss 700 in our hands) (49), which we confide can be technically solved in the near future.

4.7. Gene regulation quantification

Gene regulation of biomarkers associated with cell death, oxidative stress, and inflammation can be obtained by RT-qPCR using specific primers (2,30,65). In sodium iodate and HpODE retina degeneration, BCL1 associated X apoptosis regulator (Bax) and Bcl2 antagonists/killer (Bak) are up-regulated (2,30). Oxidative stress genes – NAPDH oxidase 1 (Nox1), Nox2, Nox3, Nox4, Dual oxidase 1 (Doux1) or Doux2 – are upregulated in sodium iodate and HpODE retinal degeneration (2; our observation). Inflammation-related genes – Tumor necrosis factor (TNF)-α, Interleukin (IL)-6, Intercellular adhesion molecule 1 (Icam1), C-C motif chemokine ligand (Ccl) 2, Ccl3, Ccl7 or Ccl8 - are also upregulated after sodium iodate treatment (65) (our observation, data not shown) and HpODE (2). An additional comment on tissue preparation is that it is also acceptable to use whole posterior eyeballs, and not separate tissues coming from either the neural retina or the RPE side, because the presence of degenerated and angiogenic tissues hinder tissue separation, and infiltrated cells between the retina and the RPE could be lost during tissue separation, which means that the associated information will be missing.

5 Discussion and Conclusions

The shortage of typical Dry AMD preclinical animal models is widely noticed. However, the recent reported laser-induced Dry AMD model (18) and the systemic, intravitreal and subretinal injection of sodium iodate (28,29,34), intravitreal and subretinal injection of lipid peroxides (2,37,38) might meet the requirement for the preclinical platform of Dry AMD models, which complimentary to the laser-induced and VEGF-A^{high} Wet AMD models (16,17). The light-damage model could also be utilized if the focus is inflammation and infiltrated microglia (61,67). Summarizing, light damage induces microglia subretinal migrationand retina thinning, sodium iodate induces RPE and retinal degeneration, and HpODE induces RPE and retinal degeneration plus CNV. Therefore, most of the clinical features expected in the human disease could be addressed using these existent models (Tables 1- 3). Among the AMD models, sodium iodate model has been most widely studied and used for the translational study, and the different dosages and administration routes of sodium iodate provides different aspects of the phenotypes. On the other hand, the sodium iodate model is acute, and might be hard to study the intermediate/progressing form of AMD, whereas HpODE AMD model is more slowly progressed than sodium iodate model and finally includes CNV. However, HpODE was only studied in *SD* rats via a route of subretinal injection and albino rabbits via a route of intravitreal injection. Thus, additional studies will be valuable for translational studies for relating human AMD progressing.

Assessment and quantification methods in preclinical studies should be further standardized and harmonized. In fact, there are still gaps in the assessment methods used by animal research and human clinical trials, because invasive methods are generally allowed in animal experiments, whereas only non-invasive assessment is applicable in clinical trials. The invasive methods in animal models, which we discussed above, are correlated with the non-invasive ophthalmic assessments, including color fundus, fundus autofluorescence (FAF) and optical coherence tomography (OCT). However, sensitivity and resolution of clinical ophthalmic assessment appears to be lower than invasive methods. Furthermore, the observations done by the non-invasive ophthalmic equipment sometimes cannot be fully explained because it is not possible to investigate the molecular and anatomical aspects, that requires the dissection of eye tissues. For example, FAF is associated with increasing lipofuscin (68), infiltrated microglia (3,69), photoreceptor rosettes (69–71) and migrating RPE cells (69), of which association can be fully dissected in the animals, but not in the human eyes. ERG functional data are considered as an earlier indicator of impaired vision and is more sensitive than the morphological changes and analyses, and ERG test protocols should be standardized for both clinical patient exams and experimental study with animal models. When patients' safety is considered, the smallest light intensity possible could be used to measure ERG response before and after a period of treatment to reduce repetitive and harmful exposures to strong light intensity. However, one final issue that needs to be always kept in mind, is that murine eyes are not human and animal disease models are not exactly alike human's, although there are many merits in animal research, which is the only mean that we have to address specific questions to the physiopathology and therapy of eye diseases.

Supplementary Material

Refer to Web version on PubMed Central for supplementary material.

Acknowledgements

We thank Drs. Dario Rusciano (Sooft Italia, Italy) and Gail Seabold (Office of Intramural Training and Education/ National Institutes of Health, US) for a critical reading of the manuscript, comments.

References

1. Wu KH, Madigan MC, Billson FA, et al. Differential expression of GFAP in early v late AMD: a quantitative analysis. Br J Ophthalmol 2003;87:1159–66. [PubMed: 12928288]
2. Kim SY, Kambhampati SP, Bhutto IA, et al. Evolution of oxidative stress, inflammation and neovascularization in the choroid and retina in a subretinal lipid induced age-related macular degeneration model. Exp Eye Res 2021;203:108391. [PubMed: 33307075]
3. Kim SY, Yang HJ, Chang YS, et al. Deletion of aryl hydrocarbon receptor AHR in mice leads to subretinal accumulation of microglia and RPE atrophy. Invest Ophthalmol Vis Sci 2014;55:6031–40. [PubMed: 25159211]
4. Combadiere C, Feumi C, Raoul W, et al. CX3CR1-dependent subretinal microglia cell accumulation is associated with cardinal features of age-related macular degeneration. J Clin Invest 2007;117:2920–8. [PubMed: 17909628]
5. Gambril JA, Sloan KR, Swain TA, et al. Quantifying Retinal Pigment Epithelium Dysmorphia and Loss of Histologic Autofluorescence in Age-Related Macular Degeneration. Invest Ophthalmol Vis Sci 2019;60:2481–93. [PubMed: 31173079]

6. Hwang JC, Chan JW, Chang S, et al. Predictive value of fundus autofluorescence for development of geographic atrophy in age-related macular degeneration. Invest Ophthalmol Vis Sci 2006;47:2655–61. [PubMed: 16723483]
7. Smith RT, Chan JK, Busuoic M, et al. Autofluorescence characteristics of early, atrophic, and high-risk fellow eyes in age-related macular degeneration. Invest Ophthalmol Vis Sci 2006;47:5495–504. [PubMed: 17122141]
8. Curcio CA, Zanzottera EC, Ach T, et al. Activated Retinal Pigment Epithelium, an Optical Coherence Tomography Biomarker for Progression in Age-Related Macular Degeneration. Invest Ophthalmol Vis Sci 2017;58:BIO211-BIO26.
9. Keenan TD, Agron E, Mares J, et al. Adherence to the Mediterranean Diet and Progression to Late Age-Related Macular Degeneration in the Age-Related Eye Disease Studies 1 and 2. Ophthalmology 2020;127:1515–28. [PubMed: 32348832]
10. Chew EY, Clemons TE, Agron E, et al. Ten-year follow-up of age-related macular degeneration in the age-related eye disease study: AREDS report no. 36. JAMA Ophthalmol 2014;132:272–7. [PubMed: 24385141]
11. Bahadorani S, Singer M. Recent advances in the management and understanding of macular degeneration. F1000Res 2017;6:519. [PubMed: 28491291]
12. Kaszubski P, Ben Ami T, Saade C, et al. Geographic Atrophy and Choroidal Neovascularization in the Same Eye: A Review. Ophthalmic Res 2016;55:185–93. [PubMed: 26871899]
13. Lois N, McBain V, Abdelkader E, et al. Retinal pigment epithelial atrophy in patients with exudative age-related macular degeneration undergoing anti-vascular endothelial growth factor therapy. Retina 2013;33:13–22. [PubMed: 22846802]
14. Wong WL, Su X, Li X, et al. Global prevalence of age-related macular degeneration and disease burden projection for 2020 and 2040: a systematic review and meta-analysis. Lancet Glob Health 2014;2:e106–16. [PubMed: 25104651]
15. Masland RH. Neuronal diversity in the retina. Curr Opin Neurobiol 2001;11:431–6. [PubMed: 11502388]
16. Shah RS, Soetikno BT, Lajko M, et al. A Mouse Model for Laser-induced Choroidal Neovascularization. J Vis Exp 2015:e53502. [PubMed: 26779879]
17. Okamoto N, Tobe T, Hackett SF, et al. Transgenic mice with increased expression of vascular endothelial growth factor in the retina: a new model of intraretinal and subretinal neovascularization. Am J Pathol 1997;151:281–91. [PubMed: 9212753]
18. Ibbett P, Goverdhan SV, Pipi E, et al. A lasered mouse model of retinal degeneration displays progressive outer retinal pathology providing insights into early geographic atrophy. Sci Rep 2019;9:7475. [PubMed: 31097765]
19. Jaadane I, Villalpando Rodriguez GE, Boulenguez P, et al. Effects of white light-emitting diode (LED) exposure on retinal pigment epithelium in vivo. J Cell Mol Med 2017;21:3453–66. [PubMed: 28661040]
20. Lin CH, Wu MR, Huang WJ, et al. Low-Luminance Blue Light-Enhanced Phototoxicity in A2E-Laden RPE Cell Cultures and Rats. Int J Mol Sci 2019;20. [PubMed: 31861461]
21. Liu RT, Gao J, Cao S, et al. Inflammatory mediators induced by amyloid-beta in the retina and RPE in vivo: implications for inflammasome activation in age-related macular degeneration. Invest Ophthalmol Vis Sci 2013;54:2225–37. [PubMed: 23462752]
22. Huang P, Sun J, Wang F, et al. MicroRNA Expression Patterns Involved in Amyloid Beta-Induced Retinal Degeneration. Invest Ophthalmol Vis Sci 2017;58:1726–35. [PubMed: 28324113]
23. Gelfand BD, Wright CB, Kim Y, et al. Iron Toxicity in the Retina Requires Alu RNA and the NLRP3 Inflammasome. Cell Rep 2015;11:1686–93. [PubMed: 26074074]
24. Rogers BS, Symons RC, Komeima K, et al. Differential sensitivity of cones to iron-mediated oxidative damage. Invest Ophthalmol Vis Sci 2007;48:438–45. [PubMed: 17197565]
25. Song D, Kanu LN, Li Y, et al. AMD-like retinopathy associated with intravenous iron. Exp Eye Res 2016;151:122–33. [PubMed: 27565570]
26. Moriguchi M, Nakamura S, Inoue Y, et al. Irreversible Photoreceptors and RPE Cells Damage by Intravenous Sodium Iodate in Mice Is Related to Macrophage Accumulation. Invest Ophthalmol Vis Sci 2018;59:3476–87. [PubMed: 30025075]

27. Zhou P, Kannan R, Spee C, et al. Protection of retina by alphaB crystallin in sodium iodate induced retinal degeneration. PLoS One 2014;9:e98275. [PubMed: 24874187]
28. Ahn SM, Ahn J, Cha S, et al. The effects of intravitreal sodium iodate injection on retinal degeneration following vitrectomy in rabbits. Sci Rep 2019;9:15696. [PubMed: 31666618]
29. Bhutto IA, Ogura S, Baldeosingh R, et al. An Acute Injury Model for the Phenotypic Characteristics of Geographic Atrophy. Invest Ophthalmol Vis Sci 2018;59:AMD143-AMD51.
30. Wang J, Iacovelli J, Spencer C, et al. Direct effect of sodium iodate on neurosensory retina. Invest Ophthalmol Vis Sci 2014;55:1941–53. [PubMed: 24481259]
31. Machalinska A, Lubinski W, Klos P, et al. Sodium iodate selectively injuries the posterior pole of the retina in a dose-dependent manner: morphological and electrophysiological study. Neurochem Res 2010;35:1819–27. [PubMed: 20725778]
32. Kim HL, Nam SM, Chang BJ, et al. Ultrastructural Changes and Expression of PCNA and RPE65 in Sodium Iodate-Induced Acute Retinal Pigment Epithelium Degeneration Model. Neurochem Res 2018;43:1010–9. [PubMed: 29569173]
33. Yang Y, Ng TK, Ye C, et al. Assessing sodium iodate-induced outer retinal changes in rats using confocal scanning laser ophthalmoscopy and optical coherence tomography. Invest Ophthalmol Vis Sci 2014;55:1696–705. [PubMed: 24526437]
34. Chowers G, Cohen M, Marks-Ohana D, et al. Course of Sodium Iodate-Induced Retinal Degeneration in Albino and Pigmented Mice. Invest Ophthalmol Vis Sci 2017;58:2239–49. [PubMed: 28418497]
35. Dysli C, Dysli M, Zinkernagel MS, et al. Effect of pharmacologically induced retinal degeneration on retinal autofluorescence lifetimes in mice. Exp Eye Res 2016;153:178–85. [PubMed: 27777124]
36. Zhang S, Zhang S, Gong W, et al. Muller Cell Regulated Microglial Activation and Migration in Rats With N-Methyl-N-Nitrosourea-Induced Retinal Degeneration. Front Neurosci 2018;12:890. [PubMed: 30559643]
37. Baba T, Bhutto IA, Merges C, et al. A rat model for choroidal neovascularization using subretinal lipid hydroperoxide injection. Am J Pathol 2010;176:3085–97. [PubMed: 20395434]
38. Armstrong D, Hiramitsu T, Gutteridge J, et al. Studies on experimentally induced retinal degeneration. 1. Effect of lipid peroxides on electroretinographic activity in the albino rabbit. Exp Eye Res 1982;35:157–71. [PubMed: 7151884]
39. Ibrahim AE, Shafaa MW, Khedr MH, et al. Comparative study between lutein and its liposomal form on cisplatin-induced retinal injury in rabbits. Cutan Ocul Toxicol 2019;38:279–85. [PubMed: 31039623]
40. Karakurt Y, Ucak T, Tasli N, et al. The effects of lutein on cisplatin-induced retinal injury: an experimental study. Cutan Ocul Toxicol 2018;37:374–9. [PubMed: 29865906]
41. Yazici A, Sogutlu-Sari E, Yay A, et al. The protective effect of selenium in cisplatin-related retinotoxicity. Cutan Ocul Toxicol 2014;33:327–32. [PubMed: 24641118]
42. Hollyfield JG, Bonilha VL, Rayborn ME, et al. Oxidative damage-induced inflammation initiates age-related macular degeneration. Nat Med 2008;14:194–8. [PubMed: 18223656]
43. Lu L, Gu X, Hong L, et al. Synthesis and structural characterization of carboxyethylpyrrole-modified proteins: mediators of age-related macular degeneration. Bioorg Med Chem 2009;17:7548–61. [PubMed: 19786352]
44. Soundara Pandi SP, Ratnayaka JA, Lotery AJ, et al. Progress in developing rodent models of age-related macular degeneration (AMD). Exp Eye Res 2021;203:108404. [PubMed: 33340497]
45. Pennesi ME, Neuringer M, Courtney RJ. Animal models of age related macular degeneration. Mol Aspects Med 2012;33:487–509. [PubMed: 22705444]
46. Ramkumar HL, Zhang J, Chan CC. Retinal ultrastructure of murine models of dry age-related macular degeneration (AMD). Prog Retin Eye Res 2010;29:169–90. [PubMed: 20206286]
47. Kannan R, Hinton DR. Sodium iodate induced retinal degeneration: new insights from an old model. Neural Regen Res 2014;9:2044–5. [PubMed: 25657718]
48. Xiao J, Yao J, Jia L, et al. Protective Effect of Met12, a Small Peptide Inhibitor of Fas, on the Retinal Pigment Epithelium and Photoreceptor After Sodium Iodate Injury. Invest Ophthalmol Vis Sci 2017;58:1801–10. [PubMed: 28346613]

49. Kim SY ZY, Kim HL, Oh Y, Xu Q. Sodium iodate-induced retina degeneration observed in non-separate sclerochoroid/retina pigment epithelium/retina whole mounts. Annals of Eye Science 2021.
50. Mones J, Leiva M, Pena T, et al. A Swine Model of Selective Geographic Atrophy of Outer Retinal Layers Mimicking Atrophic AMD: A Phase I Escalating Dose of Subretinal Sodium Iodate. Invest Ophthalmol Vis Sci 2016;57:3974–83. [PubMed: 27479813]
51. Berkowitz BA, Podolsky RH, Lenning J, et al. Sodium Iodate Produces a Strain-Dependent Retinal Oxidative Stress Response Measured In Vivo Using QUEST MRI. Invest Ophthalmol Vis Sci 2017;58:3286–93. [PubMed: 28666279]
52. Franco LM, Zulliger R, Wolf-Schnurrbusch UE, et al. Decreased visual function after patchy loss of retinal pigment epithelium induced by low-dose sodium iodate. Invest Ophthalmol Vis Sci 2009;50:4004–10. [PubMed: 19339739]
53. Jian Q, Tao Z, Li Y, et al. Acute retinal injury and the relationship between nerve growth factor, Notch1 transcription and short-lived dedifferentiation transient changes of mammalian Muller cells. Vision Res 2015;110:107–17. [PubMed: 25817714]
54. Lee SJ, Kim SY. Non-separate Mouse Sclerochoroid/RPE/Retina Staining and Whole Mount for the Integral Observation of Subretinal Layer. Bio Protoc 2021;11:e3872.
55. Kim SY, Assawachananont J. A New Method to Visualize the Intact Subretina From Retinal Pigment Epithelium to Retinal Tissue in Whole Mount of Pigmented Mouse Eyes. Transl Vis Sci Technol 2016;5:6.
56. Wunderlich KA, Tanimoto N, Grosche A, et al. Retinal functional alterations in mice lacking intermediate filament proteins glial fibrillary acidic protein and vimentin. FASEB J 2015;29:4815–28. [PubMed: 26251181]
57. Byrne LC, Khalid F, Lee T, et al. AAV-mediated, optogenetic ablation of Muller Glia leads to structural and functional changes in the mouse retina. PLoS One 2013;8:e76075. [PubMed: 24086689]
58. Steinberg RH. Interactions between the retinal pigment epithelium and the neural retina. Doc Ophthalmol 1985;60:327–46.
59. Samuels IS, Sturgill GM, Grossman GH, et al. Light-evoked responses of the retinal pigment epithelium: changes accompanying photoreceptor loss in the mouse. J Neurophysiol 2010;104:391–402. [PubMed: 20484527]
60. Kuny S, Cho WJ, Dimopoulos IS, et al. Early Onset Ultrastructural and Functional Defects in RPE and Photoreceptors of a Stargardt-Like Macular Dystrophy (STGD3) Transgenic Mouse Model. Invest Ophthalmol Vis Sci 2015;56:7109–21. [PubMed: 26529045]
61. Montalban-Soler L, Alarcon-Martinez L, Jimenez-Lopez M, et al. Retinal compensatory changes after light damage in albino mice. Mol Vis 2012;18:675–93. [PubMed: 22509098]
62. Liu Y, Li R, Xie J, et al. Protective Effect of Hydrogen on Sodium Iodate-Induced Age-Related Macular Degeneration in Mice. Front Aging Neurosci 2018;10:389. [PubMed: 30564112]
63. Zieger M, Punzo C. Improved cell metabolism prolongs photoreceptor survival upon retinal-pigmented epithelium loss in the sodium iodate induced model of geographic atrophy. Oncotarget 2016;7:9620–33. [PubMed: 26883199]
64. Hanus J, Anderson C, Sarraf D, et al. Retinal pigment epithelial cell necroptosis in response to sodium iodate. Cell Death Discov 2016;2:16054. [PubMed: 27551542]
65. Petrus-Reurer S, Bartuma H, Aronsson M, et al. Integration of subretinal suspension transplants of human embryonic stem cell-derived retinal pigment epithelial cells in a large-eyed model of geographic atrophy. Investigative Ophthalmology & Visual Science 2017;58:1314–22. [PubMed: 28241319]
66. Yunyan Ye TADD Kengo Saito, Shinmyo Yohei, Ichikawa Yoshie, Higashide Tomomi, Kagami Kyosuke, Fujiwara Hiroshi, Sugiyama Kazuhisa, Kawasaki Hiroshi. Visualization of the retina in intact eyes of mice and ferrets using a tissue clearing method. Transl Vis Sci Technol 2020;9:11.
67. Rutar M, Natoli R, Kozulin P, et al. Analysis of complement expression in light-induced retinal degeneration: synthesis and deposition of C3 by microglia/macrophages is associated with focal photoreceptor degeneration. Invest Ophthalmol Vis Sci 2011;52:5347–58. [PubMed: 21571681]

68. Sparrow JR, Duncker T. Fundus Autofluorescence and RPE Lipofuscin in Age-Related Macular Degeneration. J Clin Med 2014;3:1302–21. [PubMed: 25774313]
69. Wang NK, Lai CC, Liu CH, et al. Origin of fundus hyperautofluorescent spots and their role in retinal degeneration in a mouse model of Goldmann-Favre syndrome. Dis Model Mech 2013;6:1113–22. [PubMed: 23828046]
70. Flynn E, Ueda K, Auran E, et al. Fundus autofluorescence and photoreceptor cell rosettes in mouse models. Invest Ophthalmol Vis Sci 2014;55:5643–52. [PubMed: 25015357]
71. Secondi R, Kong J, Blonska AM, et al. Fundus autofluorescence findings in a mouse model of retinal detachment. Invest Ophthalmol Vis Sci 2012;53:5190–7. [PubMed: 22786896]
72. Marmorstein LY, Munier FL, Arsenijevic Y, et al. Aberrant accumulation of EFEMP1 underlies drusen formation in Malattia Leventinese and age-related macular degeneration. Proc Natl Acad Sci U S A 2002;99:13067–72. [PubMed: 12242346]
73. Weber BH, Lin B, White K, et al. A mouse model for Sorsby fundus dystrophy. Invest Ophthalmol Vis Sci 2002;43:2732–40. [PubMed: 12147610]
74. Yoshida T, Ohno-Matsui K, Ichinose S, et al. The potential role of amyloid beta in the pathogenesis of age-related macular degeneration. J Clin Invest 2005;115:2793–800. [PubMed: 16167083]
75. Park SW, Im S, Jun HO, et al. Dry age-related macular degeneration like pathology in aged 5XFAD mice: Ultrastructure and microarray analysis. Oncotarget 2017;8:40006–18. [PubMed: 28467791]
76. Fujihara M, Bartels E, Nielsen LB, et al. A human apoB100 transgenic mouse expresses human apoB100 in the RPE and develops features of early AMD. Exp Eye Res 2009;88:1115–23. [PubMed: 19450445]
77. Kliffen M, Lutgens E, Daemen MJ, et al. The APO(*)E3-Leiden mouse as an animal model for basal laminar deposit. Br J Ophthalmol 2000;84:1415–9. [PubMed: 11090485]
78. Dithmar S, Curcio CA, Le NA, et al. Ultrastructural changes in Bruch's membrane of apolipoprotein E-deficient mice. Invest Ophthalmol Vis Sci 2000;41:2035–42. [PubMed: 10892840]
79. Ufret-Vincenty RL, Aredo B, Liu X, et al. Transgenic mice expressing variants of complement factor H develop AMD-like retinal findings. Invest Ophthalmol Vis Sci 2010;51:5878–87. [PubMed: 20538999]
80. Hoh Kam J, Morgan JE, Jeffery G. Aged complement factor H knockout mice kept in a clean barriered environment have reduced retinal pathology. Exp Eye Res 2016;149:116–25. [PubMed: 27397653]
81. Mata NL, Weng J, Travis GH. Biosynthesis of a major lipofuscin fluorophore in mice and humans with ABCR-mediated retinal and macular degeneration. Proc Natl Acad Sci U S A 2000;97:7154–9. [PubMed: 10852960]
82. Lenis TL, Sarfare S, Jiang Z, et al. Complement modulation in the retinal pigment epithelium rescues photoreceptor degeneration in a mouse model of Stargardt disease. Proc Natl Acad Sci U S A 2017;114:3987–92. [PubMed: 28348233]
83. Vollrath D, Yasumura D, Benchorin G, et al. Tyro3 Modulates Mertk-Associated Retinal Degeneration. PLoS Genet 2015;11:e1005723. [PubMed: 26656104]
84. Karan G, Lillo C, Yang Z, et al. Lipofuscin accumulation, abnormal electrophysiology, and photoreceptor degeneration in mutant ELOVL4 transgenic mice: a model for macular degeneration. Proc Natl Acad Sci U S A 2005;102:4164–9. [PubMed: 15749821]
85. Damiani D, Alexander JJ, O'Rourke JR, et al. Dicer inactivation leads to progressive functional and structural degeneration of the mouse retina. J Neurosci 2008;28:4878–87. [PubMed: 18463241]
86. Kaneko H, Dridi S, Tarallo V, et al. DICER1 deficit induces Alu RNA toxicity in age-related macular degeneration. Nature 2011;471:325–30. [PubMed: 21297615]
87. Hahn P, Qian Y, Dentchev T, et al. Disruption of ceruloplasmin and hephaestin in mice causes retinal iron overload and retinal degeneration with features of age-related macular degeneration. Proc Natl Acad Sci U S A 2004;101:13850–5. [PubMed: 15365174]

88. Rakoczy PE, Zhang D, Robertson T, et al. Progressive age-related changes similar to age-related macular degeneration in a transgenic mouse model. Am J Pathol 2002;161:1515–24. [PubMed: 12368224]

89. Hu P, Herrmann R, Bednar A, et al. Aryl hydrocarbon receptor deficiency causes dysregulated cellular matrix metabolism and age-related macular degeneration-like pathology. Proc Natl Acad Sci U S A 2013;110:E4069–78. [PubMed: 24106308]

90. Bonilha VL, Bell BA, Rayborn ME, et al. Absence of DJ-1 causes age-related retinal abnormalities in association with increased oxidative stress. Free Radic Biol Med 2017;104:226–37. [PubMed: 28088625]

91. Zhao L, Wang Z, Liu Y, et al. Translocation of the retinal pigment epithelium and formation of sub-retinal pigment epithelium deposit induced by subretinal deposit. Mol Vis 2007;13:873–80. [PubMed: 17615538]

92. Justilien V, Pang JJ, Renganathan K, et al. SOD2 knockdown mouse model of early AMD. Invest Ophthalmol Vis Sci 2007;48:4407–20. [PubMed: 17898259]

93. Hadziahmetovic M, Song Y, Ponnuru P, et al. Age-dependent retinal iron accumulation and degeneration in hepcidin knockout mice. Invest Ophthalmol Vis Sci 2011;52:109–18. [PubMed: 20811044]

94. Ambati J, Anand A, Fernandez S, et al. An animal model of age-related macular degeneration in senescent Ccl-2- or Ccr-2-deficient mice. Nat Med 2003;9:1390–7. [PubMed: 14566334]

95. Raoul W, Keller N, Rodero M, et al. Role of the chemokine receptor CX3CR1 in the mobilization of phagocytic retinal microglial cells. J Neuroimmunol 2008;198:56–61. [PubMed: 18508131]

96. Tuo J, Bojanowski CM, Zhou M, et al. Murine ccl2/cx3cr1 deficiency results in retinal lesions mimicking human age-related macular degeneration. Invest Ophthalmol Vis Sci 2007;48:3827–36. [PubMed: 17652758]

97. Herrmann P, Cowing JA, Cristante E, et al. Cd59a deficiency in mice leads to preferential innate immune activation in the retinal pigment epithelium-choroid with age. Neurobiol Aging 2015;36:2637–48. [PubMed: 26234657]

98. Ma W, Silverman SM, Zhao L, et al. Absence of TGFbeta signaling in retinal microglia induces retinal degeneration and exacerbates choroidal neovascularization. Elife 2019;8.

99. Imamura Y, Noda S, Hashizume K, et al. Drusen, choroidal neovascularization, and retinal pigment epithelium dysfunction in SOD1-deficient mice: a model of age-related macular degeneration. Proc Natl Acad Sci U S A 2006;103:11282–7. [PubMed: 16844785]

100. Schwesinger C, Yee C, Rohan RM, et al. Intrachoroidal neovascularization in transgenic mice overexpressing vascular endothelial growth factor in the retinal pigment epithelium. Am J Pathol 2001;158:1161–72. [PubMed: 11238064]

101. Hu W, Jiang A, Liang J, et al. Expression of VLDLR in the retina and evolution of subretinal neovascularization in the knockout mouse model's retinal angiomatous proliferation. Invest Ophthalmol Vis Sci 2008;49:407–15. [PubMed: 18172119]

102. Iejima D, Nakayama M, Iwata T. HTRA1 Overexpression Induces the Exudative Form of Age-related Macular Degeneration. J Stem Cells 2015;10:193–203. [PubMed: 27125063]

103. Zhao L, Wang C, Song D, et al. Systemic administration of the antioxidant/iron chelator alpha-lipoic acid protects against light-induced photoreceptor degeneration in the mouse retina. Invest Ophthalmol Vis Sci 2014;55:5979–88. [PubMed: 25146987]

104. Tobe T, Ortega S, Luna JD, et al. Targeted disruption of the FGF2 gene does not prevent choroidal neovascularization in a murine model. Am J Pathol 1998;153:1641–6. [PubMed: 9811357]

105. Nakajima T, Hirata M, Shearer TR, et al. Mechanism for laser-induced neovascularization in rat choroid: accumulation of integrin alpha chain-positive cells and their ligands. Mol Vis 2014;20:864–71. [PubMed: 24959065]

106. Lyzogubov VV, Tytarenko RG, Liu J, et al. Polyethylene glycol (PEG)-induced mouse model of choroidal neovascularization. J Biol Chem 2011;286:16229–37. [PubMed: 21454496]

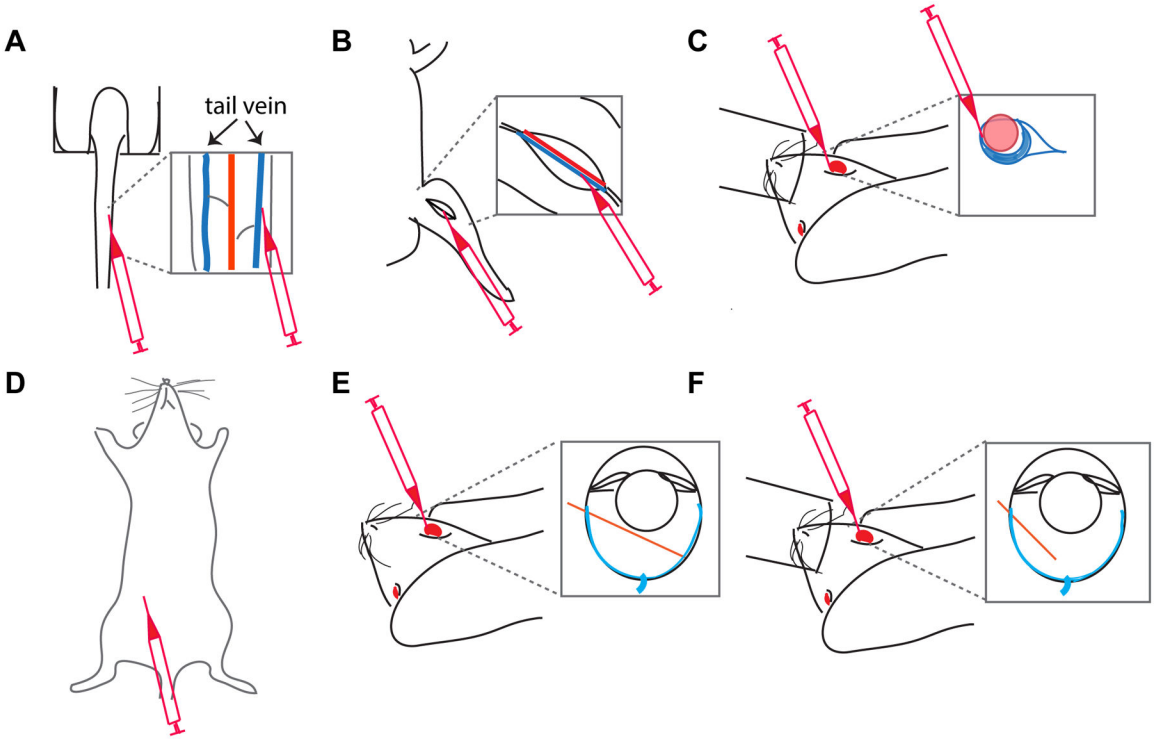

Figure 1.

Schematic diagrams illustrate chemical administration routes for tail vein (A), femoral vein (B), retro-orbital venous sinus (C), intraperitoneal (D), subretinal (E), intravitreal (F) injections.

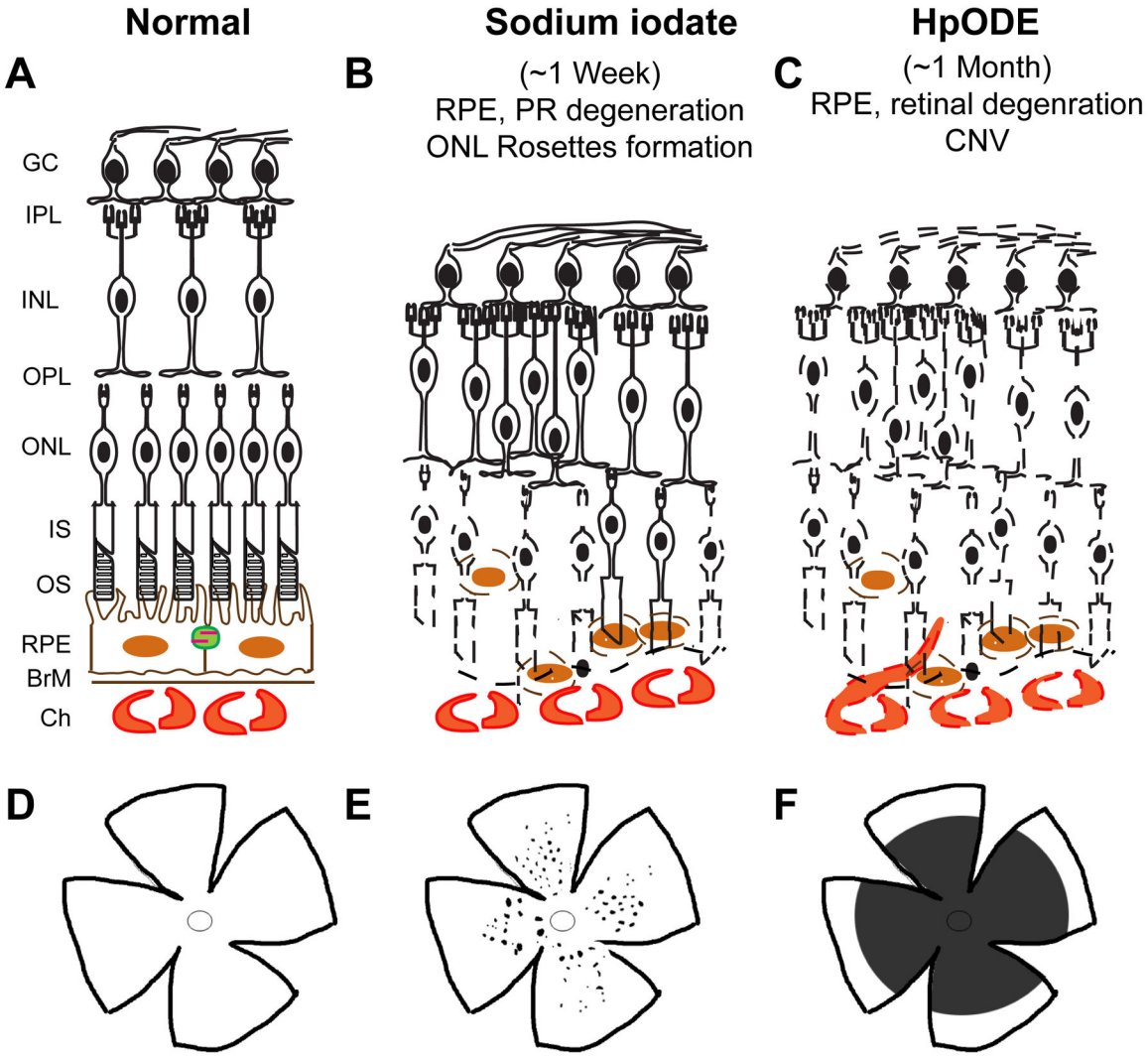

Figure 2. Schematic diagram displaying the features of retina degeneration induced by systemic/ intraperitoneal sodium iodate or subretinal HpODE injection.

Vertical (A-C) and horizontal (D-F) retinas of normal (A, D), sodium iodate (B, E) and HpODE (C, F). Black dots (E) represent rosettes and dark gray area (F) represent degenerated area. HpODE, 13(S)-hydroperoxy-9Z, 11E-octadecadienoic acid.

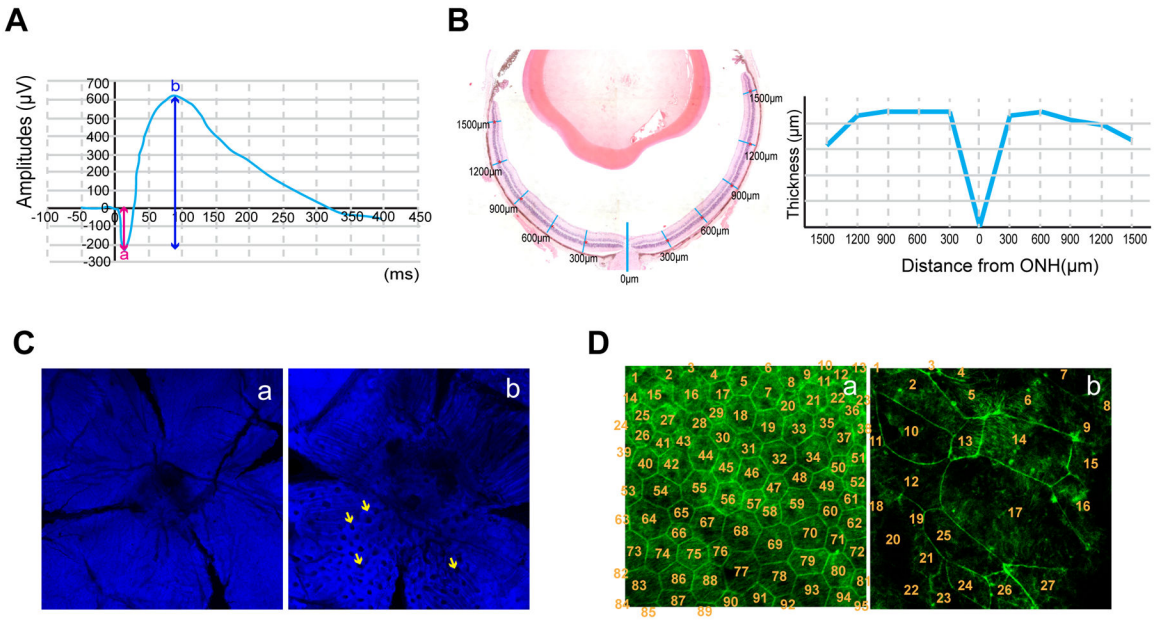

Figure 3. Evaluation methods for animal models of retinal degeneration of

(A) representative dark-adapted electroretinogram response of normal C57BL/6J mouse stimulated by 10 cd.s/m^2 light flash. The amplitude of the a-wave is measured from the baseline to the negative peak (red arrow), and the amplitude of the b-wave is conventionally measured through the negative peak of a-wave to the positive peal of b-wave (blue arrow). (B) Description of retina thickness quantification, measurable at every specific length away or a specific length away from the optic nerve head (ONH). (C) Representative images of photoreceptor nuclear layer stained by nucleus dying agents such as DAPI in sclerochoroid/RPE/retina whole mounts, normal (left) and sodium iodate (40 or 50 mg/kg). Rosettes are indicated by arrows. (D) Representative images of RPE layers stained by phallodin of normal (left) and sodium iodate treated retina (right). The numbers of phallodin-outlined RPE cells are countable. ONH, optic nerve head; RPE, retinal pigment epithelium.

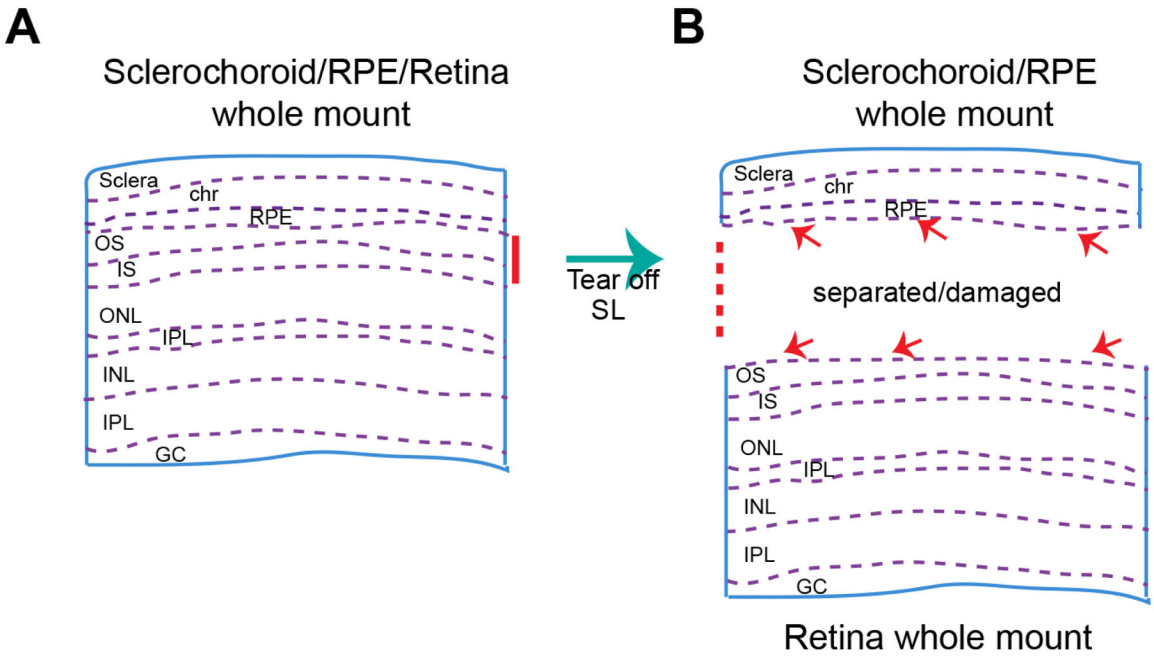

Figure 4. Description of non-separate Sclerochoroid/RPE/Retina whole mount, separate sclerochoroid/RPE and retina whole mounts.

(A) Intact subretinal layer (lined by Red) can be observed in sclerochoroid/RPE/Retina whole mount. (B) Loss/damage/separation of some information at the subretinal layer is non-avoidable at either sclerochoroid/RPE or retina whole mount. RPE, retinal pigment epithelium.

Table 1.

Genetic mice models of age-related macular degeneration

Name	Associated Function	Early AMD Lipofusin, and/or deposits	Dry AMD PR and/or RPE degeneration	Wet AMD CNV and/or contribution to CNV	Reference
EGF-Containing Fibulin-Like Extracellular Matrix Protein1 (Efemp1), R345W/R345W	genetic juvenile macular dystrophy (Doyne honecomb retinal atrophy)				Lihua et al, 2002 (72)
Timp3, S156C/S156C	genetic juvenile macular dystrophy Sorsby fundus dystrophy)				Weber et al, 2002 (73)
Neprilysin (membrane	metabolism (amyloid beta)				Yoshia et al., 2005 (74)
5XFAD	metabolism (amyloid beta)				Park et al., 2017(75)
APO B100	metabolism (lipid)				Fujihara et al 2009 (76)
*Apo*E3-Leiden*	metabolism (lipid)				Kliffen et al. 2000 (77)
APOE−/−	metabolism (lipid)				Dithmar et al. 2000 (78)
Cfh Y402H	inflammation				Ufret-Vincenty et al., 2010 (79)
Cfh−/−	inflammation				Kam et al., 2016 (80)
ATP-binding cassette transporter in rod outer segments (abcr) −/−	genetic juvenile macular dystrophy (Stargardt disease)				Maa et al., 2000 (81); Lenis et al., 2017(82)
Mertk−/−	genetic juvenile macular dystrophy (Stargardt disease)				Vollrath et al., 2015 (83)
ELOVL4	genetic juvenile macular dystrophy (Stargardt disease)				Karan et al., 2005 (84)
Dicer1−/−	metabolism (iron)				Damiani et al., 2008 (85); Kaneko et al., 2011 (86)
Ceruloplasmin (Cp)−/−/ hephaestin (Heph)-/Y	metabolism (iron)				Hahn et al. 2004 (87)
mouse cathepsin D (mcd)/mcd	metabolism (protein)				Rakoczy et al. 2002 (88)
Aryl hydrocarbon receptor (AhR)−/ −	inflammation				Hu et al., 2013 (89); Kim et al 2014 (3)
DJ1−/−	inflammation				Bonilha et al., 2017 (90)
Nuclear factor erythroid 2-related factor 2 (Nrf2) −/−	oxidative stress				Zhao et al. 2007 (91)
Superoxide dismutase (Sod)2−/−	oxidative stress				Justilien et al. 2007 (92)
Hepcidine (Hepc)−/ −	metabolism (iron)				Hadziabmetovi c et al., 2011 (93)
C-C motif chemokine ligand 2 (CCl2)−/−	inflammation				Ambati et al. 2003 (94)
C-C motif chemokine receptor 2 (CCr2)−/−	inflammation				Ambati et al. 2003 (94)

Name	Associated Function	Early AMD Lipofusin, and/or deposits	Dry AMD PR and/or RPE degeneration	Wet AMD CNV and/or contribution to CNV	Reference
C-X3-C motif chemokine receptor 1 (Cx3Cr1)−/−	inflammation				Raoul et al. 2008 (95)
CCL2−/−/Cx3Cr1−/−	inflammation				Tuo et al. 2007 (96)
CD59a−/−	inflammation				Herrmann et al., 2015 (97)
Transformting grwoth factor beta receptor (TGFbR)2−/−	inflammation				Ma et al., 2019 (98)
Sod1 −/−	Oxidative stress				Imamura et al. 2006 (99)
Rhop-Vascular endothelial growth factor (VEGF); RPE65p-VEGF	angiogenesis				Okamoto et al., 1997 (17) ; Schwesomger et a;/. 2001 (100)
Vldlr (very low-density lipoprotein receptor)−/ −	metabolism (lipid)				Hu et al., 2008 (101)
HTRA1 overexpression	inflammation				Iejima et al. 2015 (102)

The table presents mouse genetic models of AMD

Table 2.

Non-genetic age-related macular degeneration murine model

AMD form	Methods	Pathological Features	General species	Protocol
Dry	Light damage (61,67,103)	Photoreceptor degeneration; Inflammation; RPE degeneration; Oxidative stress; Subretinal microglia	*BALB/C* mouse, Sprague-Dawley rat	Fluorescent lamp, 200 to 15,000 lux, 1 hr to 24 hr, dark adaptation or not
	Blue light damage (19,20)	RPE degeneration: Oxidative stress	*Wistar, Brown Norway* rats	While (2000 lux) or blue (150 lux) light-emitting diode (LED), ~24 hr, 3 hr per day until day 21
	Amyloid beta1–40 (21,22)	Dose dependent; Inflammation; Photoreceptor degeneration; RPE degeneration	*Long-Evans* rat *C57BL/6* mouse	IVT, 5–15 μg
	Iron (23–25)	Depending on administration routes, effect or non-effect, RPE or photoreceptor damage	*C57BL/6J* mouse	i.v., IVT, subretinal
	Sodium iodate (2634,48)	Dose dependent; Administration route dependent, RPE and Photoreceptor degeneration; Photoreceptor rosettes, *Müller* glia activation, RPE movement	*C57BL/6J, 129S6/SvEvTac, BALB/C* mice, *Brown-Norway, Long-Evans, Sprague-Dawley* rats	i.v. (tail, femoral, retro-orbital), i.p., 20 to 100 mg/kg; subretinal injection, 5 μg/1 μl, 1 μl (rats)
	N-methyl-N-nitrosourea (MNU) (35,36)	Photoreceptor degeneration	*C57BL/6* mouse, *Sprague-Dawley* rat	i.p., 45, 60 mg/kg
	Carboxyethylpyrrole (CEP)-adducts (42)	Retina inflammation; Photoreceptor and RPE degeneration	*C57B/6J, BALB/C* mice	i.p., 200 μg CEP-albumin in CFA, followed 100 μg CEP-albumin in IFA
	Laser(18)	Dose dependent; Altered outer-retina; Hypo/hyper-pigmented RPE; BrM thickening, Glia activation	*C57B/6J mouse*	810 nm laser, 1.3–2.5 J/spot, 400 μm, 50 sec per spot, 5–7 spots
Dry/Wet	HpODE (2)	RPE and photoreceptor degeneration; Autofluorescence; Extended degeneration; All retinal layer defect; CNV	*Sprague-Dawley rat*	subretinal, 30 μg/2μl, 2 μl injection
Wet	Laser (16,104,105)	CNV; Inflammation; Complement activation	*C57BL/6J mouse, Brown Norway rat*	532 nm, 50–100 μm, 100–150 mW, 70 to 100 msec
	Polyethylene (PEG) (106)	CNV; Inflammation; Complement activation	*C57BL/6J mouse*	subretinal, polyethylene glycol 400, 0.5–2 mg/2μl, 2 μl injection

Abbreviations: BrM, Bruch's membrane; CFA; Complete Freurd's adjuvant; CNV, Choroidal neovascularization; ICA; Incomplete Freurd's adjuvant; i.v., Intravenous injection; IVT, Intravitreal injection; RPE, Retinal pigment epithelium

Table 3.

Observed phenotypic features of retina degeneration induced by sodium iodate according to the injection routes.

Injection routes	Species	Injection amounts	Observed features	Reference
Retro-orbital	*C57BL/6J* mouse	20, 30 mg/kg	RPE and photoreceptor degeneration; AF in fundus; Hyperreflective spots in vitreous and retina of OCT	Wang et al., 2014 (30)
i.v.	*C57BL/6J* mouse	40 mg/kg	RPE degeneration; Reduced ERG; Macrophage infiltration, Peak time of TUNEL positive RPE cells at 14 hr after injection; Peak TUNEL positive ONL at 3 D after injection; AF in fundus; Fluorescein leak choroidal degeneration; Recovered phenotypes at 4 weeks	Moriguchi et al., 2018 (26)
	Sprague-Dawley rat	40 mg/kg	RPE degeneration; Photoreceptor degeneration; Rosettes; Reduced ERG	Yang et al., 2014 (33)
i.p.	*C57BL/6J, BLAB/C* mouse	50 mg/kg	Better ERG responses in *BLAB/C* than *C57BL/6J*; More distinct AF spots in OCT and Fundus in *BLAB/C* than *C57BL/6J;* No distinct differences in histology; No distinct differences in immunofluorescent staining: ZO-1, RPE65, Rhodopsin, Blue opsin between *C57BL/6J* and *BLAB/C*	Chowers et al., 2017 (34)
	Long-Evans rat	50 mg/kg	RPE degeneration; Photoreceptor degeneration; Outer and inner retina disorganization; Muller glia activation and proliferation, Muller neurogenesis; Neurogenesis	Jian et al., 2015 (53)
	Sprague-Dawley rat	50 mg/kg	RPE and photoreceptor degeneration; Rosettes; Regeneration of RPE (PCNA and RPE65 double positivity at D3 and PCNA immunoreactivity in RPE and choroid layer at D5 and D7), Regeneration of photoreceptor (PCNA immunoreactivity in ONL)	Kim et al., 2018 (32)
Subretinal	*Brown-Norway* rat	5 μg/ul, 1 μl injection	Focal RPE and photoreceptor degeneration; Muller glia activation; Choricocapillaris degeneration	Imran et al., 2018 (29)
	Pig	1 μg, 50 μg, 100 μg, 100 μ injection	1 μg: Focal RPE and photoreceptor degeneration, 50–100μg: All retinal layers defected	Mones et al. 2016 (50)
Intravitreal	*New Zealand white* rabbit	300, 400 μg, 50 μl injection	Retinal degeneration; No RPE defect	Ahn et al., 2019 (28)

Abbreviations: AF, Autofluorescence; D, Day; ERG, Electroretinogram; i.p., Intraperitoneal injection; i.v., Intravenous injection; OCT, Optical coherence tomography; ONL, Outer nuclear layer; PCNA, Proliferating cell nuclear antigen; RPE, Retinal pigment epithelium

Table 4.

Phenotypic features of retina degeneration induced by lipid peroxides injection.

Species	Injection routes	Lipid hydroperoxides	Injection amounts	Observed features	References
New Zealand white rabbit	intravitreal	Linoleic acid hydroperoxide	19 mg	Non-recordable level of ERG responses of a and b waves by 7 days post- injection	Armstrong et al., 1982 (38)
		Linolenic acid hydroperoxide	19 mg	Non-recordable level of ERG responses of a and b waves by 20 days post-injection	
		Arachidonic acid hydroperoxide	19 mg	Reduced but maintained/recovered ERG responses of a and b waves by 20 days post-injection	
	l	Docosahexaenoic acid hydroperoxide	19 mg	Non-recordable level of ERG responses of a and b waves by 20 days post-injection	
Sprague-Dawley rat	subretinal	13(S)-hydroperoxy-9Z, 11E-octadecadienoic acid (HpODE): Linoleic acid hydroperoxide	30 μg	CNV by 3 weeks post-injection	Baba et al., 2010 (37)
Sprague-Dawley rat	subretinal	13(S)-hydroperoxy-9Z, 11 E-octadecadienoic acid (HpODE): Linoleic acid hydroperoxide	30 μg/2 μl, 2 μl injection	Extended retina degeneration, RPE degeneration, autofluorescence, oxidative stress, inflammation, CNV by 3 weeks post-injection	Kim et al., 2021 (2)

Abbreviations: CNV, Choroidal neovascularization; ERG, Electroretinogram

Table 5.

Compound summary of sodium iodate and HpODE

Name	CID	Structure	Molecular Formula	Synonyms	MW	Safety
Sodium iodate	23675764	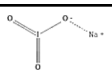	$NaIO_3$	Natriumjodat	197.9 g/mol	Oxidizer, Irritant, Health Hazard
HpODE	5280720	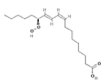	$C_{18}H_{32}O_4$	13-L-Hydroperoxylin oleic acid	312.4 g/mol	Health Hazard

Information from PubChem

Sodium iodate and HpODE are health hazard. Please check and read the Safety data sheets of them.

Abbreviations: HpODE, 13(S)-hydroperoxy-9Z, 11E-octadecadienoic acid; MW, Molecular weight

Table 6.

Calculation of i.p. injection amount of sodium iodate solution.

Make 2 mg/ml SI solution from stock 20 mg/ml with saline		
SI injection amounts	**Rats**	**Mice**
50 mg/kg	5 mg/100 g; 2.5 ml (2 mg/ml) / 100 g	0.5 mg/10g; 250 μl (2 mg/ml) / 10 g
40 mg/kg	4 mg/100 g; 2 ml (2 mg/ml) / 100 g	0.4 mg/10g; 200 μl (2 mg/ml) / 10 g
20 mg/kg	2 mg/100 g; 1 ml (2 mg/ml) / 100 g	0.2 mg/10g; 100 μl (2 mg/ml) / 10 g
10 mg/kg	1 mg/100 g; 0.5 ml (2 mg/ml) / 100 g	0.1 mg/10g; 50 μl (2 mg/ml) / 10 g

Abbreviation: i.p., Intraperitoneal injection

Table 7.

Materials for HpODE subretinal injection

Material items	Available company and cat #	Additional information
Rats	*Sprague Dawley*	6–8 weeks, 150–250 g
HpODE	Cayman Chemical (cat #, 48610–500 μg)	Ethanol evaporated, and sodium borate solution added.
Boric acid	Sigma-Aldrich (cat#, B6768–500 g)	0.02 M Sodium borate buffer (pH 9)
Injector	Harvard Apparatus, PL1–100A pico-liter microinjector,	N/A
Thin wall glass capillaries	World Precision Instruments, TW100–4	Tip internal diameter 25 to 30 μm, 100 mm glass capillaries; www.wpiinc.com
Flaming Micropipette Puller	Sutter Instrument Co. Model P-80 Brown,	Heat 950, Pull 44, Velocity 30, Time 70; www.sutter,com
Razor	Any razor is fine.	N/A
Anesthetized solution	Ketamine (KetaVed, 100 mg/ml) and Xylazine (VEDCO, 100 mg/ml)	Check the concentration of solutions available. Depending on region and country, the concentrations are different.
Ocular lubricant ointment	Alcon, Duratears	Protect non-surgery eye during the anesthesia
Dilation solution	Tropicamide (1% Mydricayl, Alcon); Mydfrin (2.5% phenylephrine hydrochloride, Alcon)	Use available dilation solution depending on country and local region.
Topical anesthetized solution	0.5% Proparacaine hydrochloride (Alcaine, Alcon); tetracaine	Use available topical anesthetized solution, depending on countries and local region; Proparacaine is less toxic than tetracaine.
Gonio solution	Hydroxypropyl methylcellulose gel (2.5% Gonak, Akorn)	When the micropipette is injected into eyeball, Gonio solution should be added to see the retina inside.
Balanced salt ophthalmic solution (BSS)	Alcon, NDC0065–0795-15	N/A
Forceps	McPherson, strait 5 mm, smooth 10.8 CM	Any blunt and safe forceps available.
Scissors	Proper scissors to remove whiskers	N/A
Needles	30 ½ gauge	N/A
Antibiotic eye drops	Ofloxacin 3mg/ml	Ocuflox eye drops can be applied before ointments. Choose proper one depending on country and region
Antibiotic ointments	PREG-G-gentamycin, prednisolone acetate suspension (Allergan Inc); Neomycin and polymyxin b sulfates and bacitracin zinc ophthalmic ointment (Akorn, Inc)	Terramycin ophthalmic ointment (Pfizer) can be applied. Depending on region and country, available commercial ophthalmic antibiotics are different.
Ear punches	Kent Scientific Corporation, Nail- Clipper	N/A
Sterile Swab	Fisherbrand cat #. 23–400-116	N/A